Modeling defoliation as a proxy for tree health: A case study on Pinus Radiata trees using machine-learning and hyperspectral data

Patrick Schratz[a], Jannes Muenchow[a], Eugenia Iturritxa[1], Alexander Brenning[a]

[a]*Department of Geography, GIScience group, Grietgasse 6, 07743, Jena, Germany*

Abstract

Keywords: hyperspectral imagery, forest health, machine-learning, variable importance, model comparison

1. Introduction

Data retrieved from remote sensing satellites is successfully used in forestry to monitor temporal changes across large areas (Martinez del Castillo et al., 2015; Sexton et al., 2015). The use of Synthetic Aperture Radar (SAR) techniques enables scientists to estimate Above-Ground Biomass (AGB) (Lu et al., 2016; Sinha et al., 2015). Forest health is commonly assesed using optical data from multi-/hyperspectral satellites by applying temporal change detections (Zhang et al., 2016). With the recent success story of machine-learning methods in the field of remote sensing, modeling techniques such as Random Forest (RF) are frequently used to model relationships of possible triggers to forest health (Belgiu & Drăguţ, 2016; Lary et al., 2016; Michez et al., 2016).

With a robust model, predictions to large areas can be conducted, providing valuable information about the health condition of forest stands. One approach to model forest health is to extract information from spectral signatures of affected and unaffected trees (Lelong et al., 2010). Spectral (vegetation-)indices

*Corresponding author
Email address: patrick.schratz@uni-jena.de (Patrick Schratz)

have shown the potential to provide valuable information to increase predictive accuracy of forest pathogens (Jiang et al., 2014; Adamczyk & Osberger, 2015).

However, the amount of possible (vegetation-)indices that can be calculated is often limited due to a low spectral resolution of freely available data from optical multispectral sensors (e.g. Sentinel-2). Also, there is currently no freely available data from hyperspectral sensors that could be used for such studies (after the decommission of the EO-1 Hyperion satellite). If the spatial resolution of the data is too coarse (e.g. $> 5m$), the value of a pixel usually contains information from multiple trees and possibly even bare-ground information. This point makes it impossible to use data from sensors like Sentinel-2 to train a model on a tree level.

In this study we will use hyperspectral data with a spatial resolution of one meter and 126 spectral bands to model the health status of Monterey Pine (*Pinus radiata*) plantations in northern Spain (Figure 1). The trees in the study area suffer from infections of invasive pathogens such as *Diplodia sapinea*, *Fusarium circinatum Armillaria mellea* or *Heterobasidion annosum* leading to a spread of cankers or defoliation (Mesanza et al., 2016; Iturritxa et al., 2017). In-situ measurements of defoliation on a tree level have been collected to serve as the response variable (as a proxy for tree health). The fungi are assumed to infect the trees through open wounds, possibly caused by previous hail damage (Iturritxa et al., 2014). The dieback of these trees, which are mainly used as timber, causes high economic damages (Ganley et al., 2009). Hyperspectral remote sensing data in combination with state-of-the-art machine-learning techniques is used to help monitoring the health status in this region by early detecting affected trees/plots. The aim is to spatially predict the fitted model to other plots/the whole Basque Country to create a forest health map.

To extract the most information from the available remote sensing data, we not only calculated the most common vegetation indices like *NDVI* to link against defoliation but all possible ones within the spectral region of the data (400 nm - 1000 nm) that are implemented in the *hsdar* package in R (Lehnert et al., 2018). Additionally, all possible combinations of Normalized Ratio Indices

(NRI) were calculated from the data and supplied to a selection of different algorithms (*Support Vector Machines (SVM)*, *Ridge Regression (RR)*, *xgboost*) as predictors.

Specifically the following objectives are addressed:

- Comparison of multiple algorithms on their performance to model defoliation of *Pinus radiata* trees using highly-correlated indices
- Exploration of the most important indices of the best performing model
- Spatial prediction of defoliation to *Pinus radiata* plots and the whole Basque Country

2. Data and study area

2.1. In-situ data

The *Pinus radiata* plots of this study, namely *Laukiz 1*, *Laukiz 2*, *Luiando* and *Oiartzun*, are located in the northern part of the Basque Country (Figure 1). *Oiartzun* has the most observations (n = 529) while *Laukiz 2* has the largest area size (1.44 ha). All plots besides *Luiando* are located nearby the coast (Figure 1). In total 1750 observations are available (*Laukiz 1* = 479, *Laukiz 2* = 451, *Luiando* = 291, *Oiartzun* = 529). The data was surveyed in September 2016.

2.2. Hyperspectral data

The airborne hyperspectral data was acquired during two flight campaigns on September 28th and October 5th 2016, both around 12 am. The images were taken using a AISAEAGLE-II sensor. All preprocessing steps (geometric, radiometric, atmospheric) have been conducted by the Institut Cartografic i Geologic de Catalunya (ICGC). The first four bands are corrupted, leaving 122 bands with valid information. Additional metadata information is available in Table 1:

Table 1: Specifications of hyperspectral data.

Characteristic	Value
Geometric resolution	1 m
Radiometric resolution	12 bit
Spectral resolution	126 bands (404.08 nm - 996.31 nm)
Correction:	Radiometric, geometric, atmospheric

3. Methods

For all analysis steps we used the open-source statistical programming language R (R Core Team, 2017). The algorithm implementations of the following packages have been used: *xgboost* (Chen & Guestrin, 2016) (*xgboost*), *kernlab*

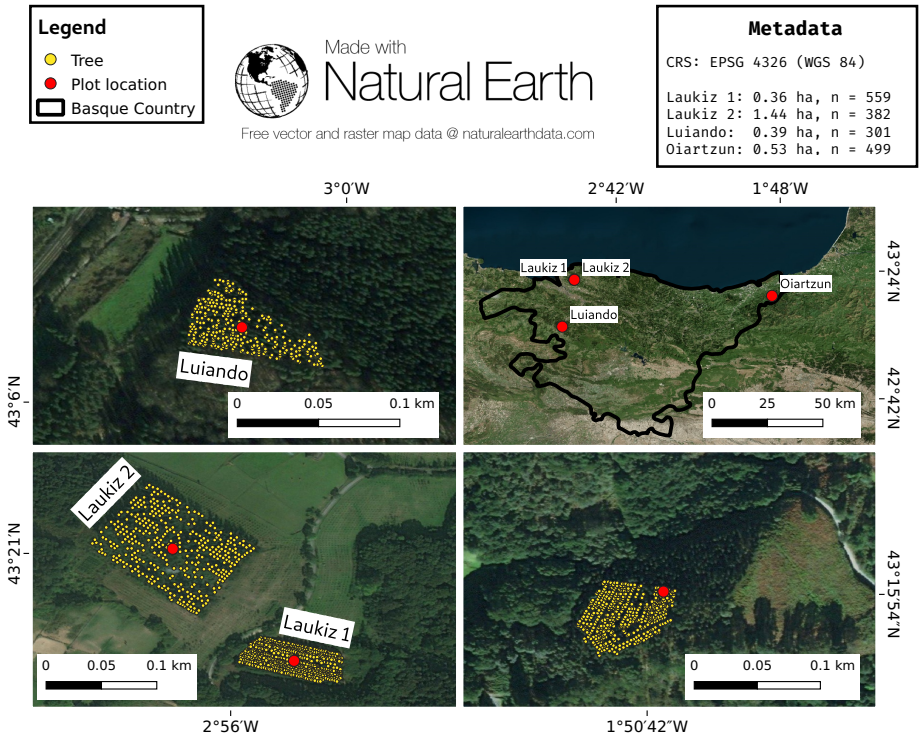

Figure 1: Information about the plot locations, the area of hyperspectral coverage and the number of trees per plot.

(Karatzoglou et al., 2004) (Support Vector Machine) and *glmnet* (Friedman et al., 2010) (Ridge Regression). We used the R package *mlr* for all modeling related steps. It provides a standardized interface for a wide variety of statistical and machine-learning models in R simplifying essential modeling tasks such as hyperparameter tuning, model performance evaluation and parallelization (Bischl et al., 2016).

3.1. Derivation of indices

To use the full information from the hyperspectral data, we not only calculated all possible vegetation indices that are available in the *hsdar* package (90 in total) but also all possible combinations of NRI. We were interested if NRIs of arbitrary band combinations will have a substantial positive effect on the predictive power of the fitted model. The NRI were calculated using the following formula:

$$NRI_{i,j} = \frac{b_i - b_j}{b_i + b_j} \tag{1}$$

where i and j are the respective band numbers.

To account for geometric offsets (which were reported with up to 1 m), we used a buffer of two meters around the centroid of the respective tree. The mean value of all pixels touched by the buffer was assigned as the final value for each index. Missing values were removed from the mean value calculation. In total, 7875 Normalized Ratio Indices NRI were calculated ($\frac{125*126}{2}$). Due to four corrupted bands and other numerical problems, some indices returned `NA` for specific observations. These indices were removed from the dataset, leaving a total of 7471 variables without missing values.

3.2. Benchmarking of algorithms

Three algorithms (*xgboost*, *SVM*, *RR*) were benchmarked on predictive performance. Besides the well-known SVM algorithm (Vapnik, 1998) we also used *xgboost* which is ensemble method relying on the idea of tree boosting that

gained a lot of attention in recent years (Chen & Guestrin, 2016). We also added penalized L2 (Ridge) regression to the portfolio due to its ability to handle highly correlated covariates (REFERENCE). The probably most popular machine-learning algorithm, Random Forest (Breiman, 2001), was not considered for this study: Due to the high number of variables, model fitting times in the range hours for a single model fit were not practicable for this work. These high fitting times are caused by hyperparameter `mtry` which scales with the number of variables (Probst et al., 2018). After the selection of the best model, we checked if the winning algorithm can achieve a similar performance when using only the most important variables compared to using all variables. This would simplify the spatial prediction a lot as less indices need to be computed from the data used for prediction. Also, simpler models are always preferred over complex ones (REFERENCE).

3.2.1. Performance estimation

The algorithms were benchmarked in two ways: 1) Using spatial block cross-validation (CV) on the plot level with each plot serving as the test set once. This approach results in four performance estimates, one for each fold. 2) Using five-fold five-times repeated spatial CV for each plot based on the k-means clustering approach of Brenning (2012). As the best algorithm of 1) will be used for the spatial prediction, we first conducted the model selection on this setup and only applied the winning algorithm on 2).

3.2.2. Hyperparameter tuning

To tune the hyperparameters of the algorithms, we used Sequential-based Model Optimization (SMBO) via the R package *mlrMBO* (Bischl et al., 2017). This Bayesian approach first composes n randomly chosen hyperparameter settings out of a user defined search space. After these n tries have been evaluated, a new hyperparameter setting which is going to be evaluated next is proposed based on a surrogate model. This strategy continues until a termination criterion, defined by the user, is reached (Hutter et al., 2011; Jones et al., 1998). In this work we

used an initial design of 30 randomly composed hyperparameter settings and a termination criterion of 20 iterations, resulting in a total budget of 50 evaluated hyperparameter settings per fold. The advantage of this tuning approach is that it substantially reduces the tuning budget which is needed to find a setting close to the global minimum compared to methods that do not use information from previous runs such as *random search* or *grid search* (Bergstra & Bengio, 2012).

3.3. Variable importance

To find indices that contributed most to model performance, we used the internal variable importance measure of the *xgboost* algorithm. The score is calculated by taking the contribution of each feature for each tree in the fitted model. The higher the score of a variable, the more important it is for the fitted model when making predictions (Chen & Guestrin, 2016). The variable importance measure is automatically computed during model fit. In contrast to other approaches such as permutation-based ones, the *xgboost* score is composed out of three parts that contribute to the overall importance (Chen & Guestrin, 2016):

- Gain: The relative contribution of the feature to the model
- Cover metric: How often a feature was selected to be the deciding feature in a tree for a specific observation
- Frequency How often a feature occurs in all trees of the model

The *Gain* features is the most important one among the three. All measures sum up to one (Chen & Guestrin, 2016).

4. Results

4.1. Plot characteristics

Oiartzun shows the highest defoliation ($\bar{x} = 69.22\%$) among the plots while *Laukiz 2* is the healthiest ($\bar{x} = 13.54\%$) (Figure 2). All plots besides *Luiando* show an evenly distributed level of defoliation across the entire plot.

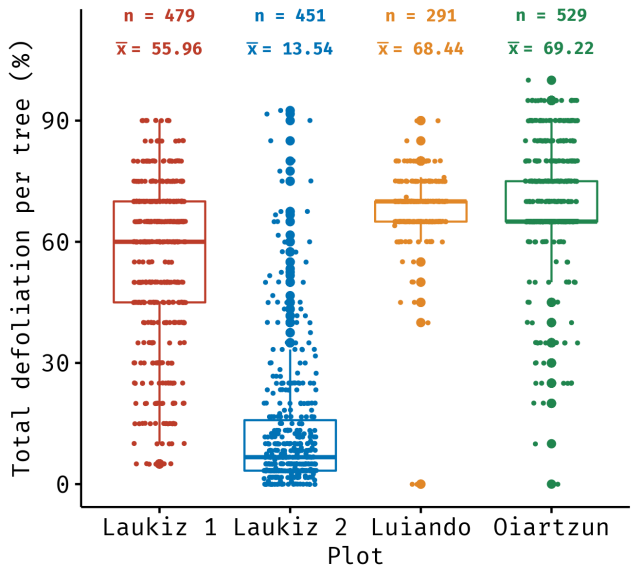

Figure 2: Descriptive statistics of the response variable *defoliation*.

Table 2: Four-fold block spatial CV performances of RR, SVM and xgboost using RMSE as the error measure. Mean and standard deviation are shown.

RR	SVM	xgboost	xgboost (7 variables)
59.10 (22.71)	36.23 (15.73)	33.26 (16.61)	

The high overall degree of defoliation of *Luiando* and *Oiartzun* is also visible in the spectral signatures of the plots (Figure A.7). Both plots show lower mean reflectance values around the wavelength range 800 nm - 1000 nm compared to Laukiz 1 and Laukiz 2. *Oiartzun* is almost completely missing the reflectance drop at around 815 nm that is visible for all other plots but instead shows a higher magnitude for the reflectance increase at around 920 nm. *Laukiz 2* shows a mean tree density of 61.59 m (Figure 3) while all other plots are more dense (34.64 m (Laukiz 1), 33.01 m (Luiando), 34.96 m (Oiartzun)) (Figure 3).

Table 3: Predictive performance of *xgboost* using all observations and all variables (All Observations/all variables), all observations and the seven most important variables only (All Observations/7 variables) and observations from specific plots only (Plot level observation/all variables) with RMSE as the error measure. The performance estimates for "All Observations" correspond to the fold for which the respective plot was serving as the test set. Column "Plot level observation", shows the mean RMSE estimates at the repetition level of a five-fold five-times repeated spatial CV, scored by using data of the respective plot only.

Plot/Data	All Observations/ all variables (Block CV)	All Observations/ 7 variables (Block CV)	Plot level observations/ all variables (SpCV)
Laukiz 1	22.03	21.47	19.18
Laukiz 2	51.75	49.94	17.24
Luiando	13.20	15.37	8.30
Oiartzun	32.97	17.62	14.40

4.2. Predictive performance

4.2.1. Algorithm benchmarking

The *xgboost* algorithm showed the lowest error (33.26 RMSE) when benchmarking the learners on the complete dataset of all plots (Table 2). While the *SVM* performance was only slightly worse (36.23 RMSE), *RR* showed a substantially worse performance than *xgboost* (59.10 RMSE).

4.2.2. Single models vs. super model

When comparing the mean predictive performance of models fitted at the plot level against the performance of the model that was fitted using all data (super model), the plot-level models showed a better performance in all cases (Table 3). The highest difference between both model types occurred for plot *Laukiz2* with a difference of 34.51 RMSE.

Using only the seven most important variables (Figure 4) for the super model showed small increases in performance for *Laukiz 1* and *Laukiz 2*, a small decrease for *Luiando* and almost a reduction of 50% of the error for *Oiartzun* (32.97 vs. 17.62 RMSE) (Table 3).

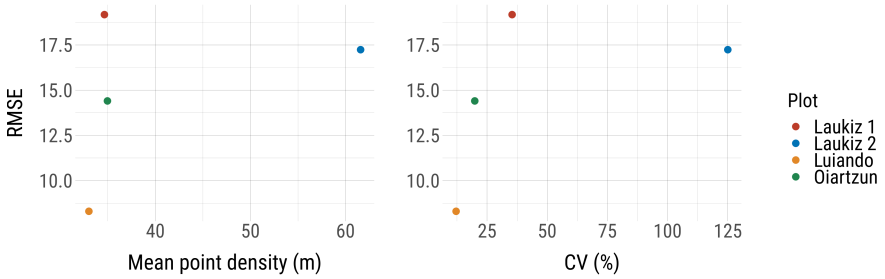

Figure 3: RMSE vs. mean point density and coefficient of variation (defoliation).

4.2.3. RMSE vs. plot characteristics

An increase of the error rate was observed with an increase of descriptive plot measures such as mean point density and the coefficient of variation (based on the response variable *defoliation*) (Figure 3).

4.3. Variable importance

The seven most important features of the super model in this study were vegetation indices with the *EVI* (Huete et al., 1997) being the most important one (Figure 4).

$$EVI = 2.5 * \frac{R_{800} - R_{670}}{R_{800} - (6 * R_{670}) - (7.5 * R_{475}) + 1)} \tag{2}$$

where R = Reflectance at the respective wavelength.

Vegetation index *GDVI* appears three times among the first seven most important features (Figure 4) with different `n` values. This is because it was computed four times, with `n` ranging from 1 - 4 (Wu et al., 2008):

$$GDVI = \frac{R^n_{800} - R^n_{680}}{R^n_{800} + R^n_{680}} \tag{3}$$

The seven most important features (*EVI*, *GDVI4*, *D1*, *GDVI3*, *GDVI2*, *mNDVI* and *mSR*) show a substantial difference in the importance score compared to all following variables (Figure 4).

Table 4: Formulas of the five most important vegetation indices of the super model. R = Reflectance at wavelength, D = First derivation of reflectance value at wavelength.

Acronym	Name	Formula	Reference
EVI	Enhanced vegetation index	$2.5 * \frac{R_{800}-R_{670}}{R_{800}-(6*R_{670})-(7.5*R_{475})+1)}$	Huete et al. (1997)
GDVI	Generalized DVI*	$\frac{R^n_{800}-R^n_{680}}{R^n_{800}+R^n_{680}}$	Wu et al. (2008)
D1	Derivative Index	$\frac{D_{730}}{D_{706}}$	Zarco-Tejada et al. (2003)
mNDVI	Normalized DVI*	$\frac{R_{800}-R_{680}}{(R_{800}+R_{680}-2*R_{445}}$	Sims & Gamon (2002)
mSR	Simple Ratio Index	$\frac{R_{800}-R_{445}}{R_{680}-R_{445}}$	Sims & Gamon (2002)

* Difference Vegetation Index

The best NRI scored rank eight (band 112 and band 62). All further places up to rank 30 are NRIs.

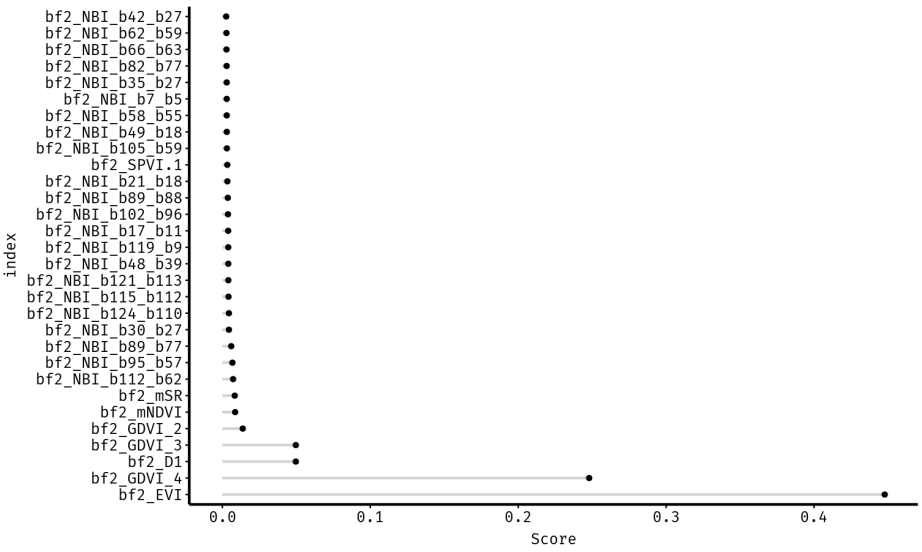

Figure 4: The 30 most important variables as estimated by the internal variable importance measure of the *xgboost* algorithm. The higher the score, the more important the feature. "bf2" notes that a buffer of 2 meter was used to extract the variable information to the tree observation. "NRI" means that a normalized ratio index with the subsequent bands was calculated. Features without "NRI" prefix are vegetation indices, e.g. "bf2_EVI".

.

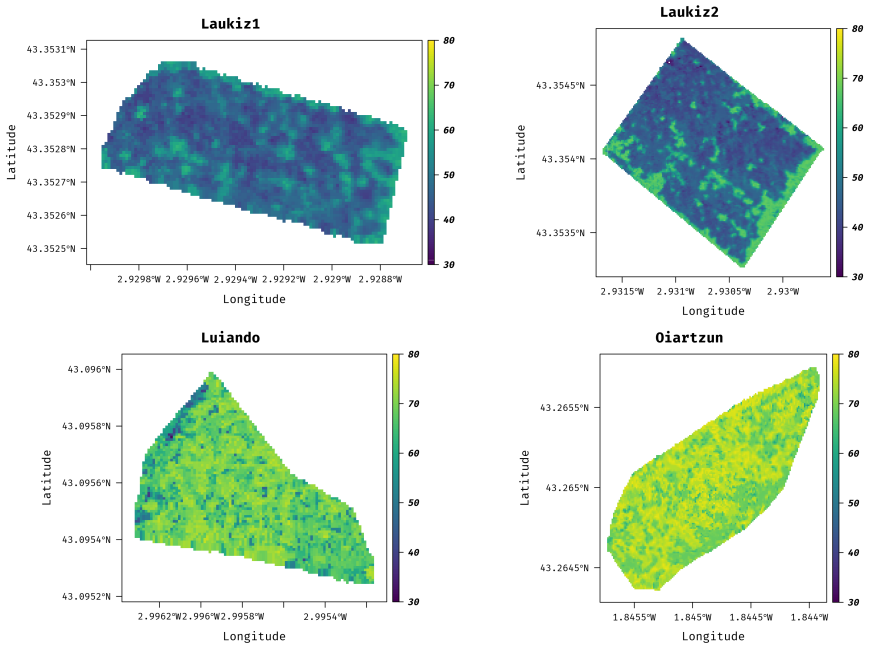

Figure 5: Spatially predicted defoliation (in %) from *xgboost* of *Laukiz 1*, *Laukiz 2*, *Luiando* and *Oiartzun*.

4.4. Spatial prediction

The plots with a higher mean defoliation (*Luiando* and *Oiartzun*) showed a good visual separability compared to the healthier plots *Laukiz 1* and *Laukiz 2* (Figure 5). All predicted values ranged between 30 % and 80 % with *Luiando* showing the smallest variance (Figure 6).

The high error of the super model for *Laukiz 2* (49.94 RMSE) is also visible in the respective histogram as most predictions range between 40 % - 50 % (Figure 6) while in fact most trees of *Laukiz 2* show an actual defoliation of around 20 % (Figure 2).

For the less defoliated plots *Laukiz 1* and *Laukiz 2* a subtle level of separation between trees and bare ground is visible (Figure 5). This is not the case for the other two higher defoliated plots for which bare ground and defoliated predictions are mainly in the same value range (around 60 % - 80 %).

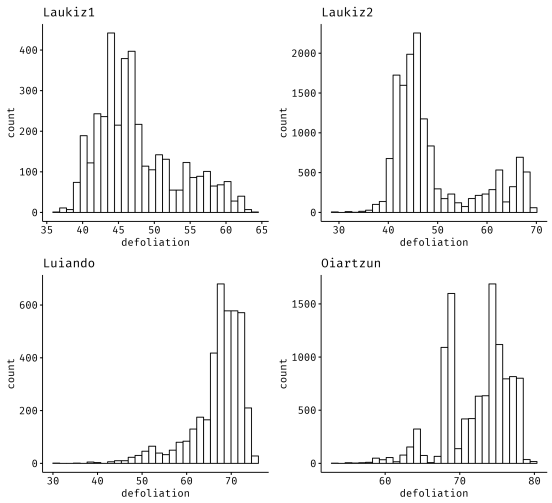

Figure 6: Histograms of predicted defoliation (in %) from *xgboost* of *Laukiz 1*, *Laukiz 2*, *Luiando* and *Oiartzun*.

[ADD FIGURE WITH SENTINEL2 PREDICTION]

5. Discussion

5.1. Derivation of indices

The buffer of 2 m that we used to generate the index value for each observation can be seen critical. When using no buffer at all, the possibility is high that a pixel value gets assigned to the tree observation that does not spatially match. Using a buffer of more than 2 meters would increase the probability of merging information from other trees into the pixel value, blurring the actual value of the tree observation. Thats why in our view using a buffer of 2 m was the best compromise here.

The exact number of contributing pixels to the final index value of an observation cannot be determined as it depends on the location of the tree within the pixel grid. As the buffer is a circle, it depends on the exact location of a tree observation within a pixel how much surrounding pixels are touched by the circle that will then be used to calculate the final pixel value. If a tree observation

is located at the border of the plot, some directions of the buffer will contain no values and the subsequent index value will be calculated using less pixels than if the tree observation is located in the middle of the plot.

Using a buffer in the first place and the fact that it is unclear how much information from other trees went into the calculation of an index value of a certain observation introduced a bias of an unknown magnitude into the data. This has to be considered when making interpretations about the outcome of this study.

5.2. RMSE vs. plot characteristics

Relating the modeling error to plot characteristics (mean point density, coefficient of variation) did not show a clear picture: For both comparisons, *Laukiz 2* did not follow the pattern that was observed from the other three plots (Figure 3) of having an increase in error with an increase in mean point density and coefficient of variation.

It needs to be considered that we only looked at four plots in this work. To make a robust statement about a possible relationship between modeling error and plot characteristics, a larger sample size of plots is needed.

5.3. Predictive Performance

5.3.1. Algorithm benchmarking

The relatively large difference in performance between *RR* (59.10 RMSE) and the machine-learning models (36.23 and 33.26 RMSE) is remarkable. *RR* has shown promising performance results in other studies when many highly-correlated predictors were involved (REFERECES). However, in this study, *RR* was not able to achieve a sufficient performance score compared to *SVM* and *xgboost* even though its hyperparameter λ was properly tuned using SMBO.

While *xgboost* shows a slightly better performance than *SVM*, the latter has the advantage of only having two hyperparameters that need to be tuned. This results in a shorter runtime. Nevertheless, *xgboost* showed the best performance

and was subsequently selected to fit the models on the plot level and for the spatial prediction.

An important point that needs to be considered when interpreting the performance results is that we only related defoliation to indices derived from remote sensing data. Possible other local variables that could help in predicting defoliation were not considered. One example here is tree age: The older a tree the more vulnerable it may be to pathogen infections causing defoliation. However, such predictors would not be available for a spatial prediction scenario and one of the main goals of this study is to relate defoliation to variables that are available on a larger scale (e.g. remote sensing indices).

5.3.2. Single models vs. super model

It is expected that models that were trained on the plot level only achieve a better performance than the global model. The low performance on Laukiz 2 for the super model is most likely due to the difference of this plot to all others: The fitted model on Laukiz 1, Luiando and Oiartzun is not capable of reaching a good performance on the Laukiz 2 prediction data. This is not surprising as Laukiz 2 shows substantially different plot characteristics compared to all others plots in terms of the distribution of the response variable *defoliation* (Figure 2) and the mean point density of trees (Figure 3).

The low error for Luiando (8.30 RMSE) for the plot model validates the approach of relating defoliation to vegetation indices and NRI. The overall error of the super model (33.26 RSME) is expected to decrease if more plots are available for training. To reach an optimal performance, the fitted model would need to include at least one instance of every plot that shows unique characteristics (i.e. here Laukiz 2 is substantially different to the others). Possibly more plots showing unique characteristics exists that are not integrated into the fitted model of this work.

An interesting find is that the supermodel with only seven variables shows a better overall performance than the model with all 7471 variables (Table 3). This leads to the conclusion that adding as many variables as possible to a model

will not necessarily improve its performance. In contrast, too much information can even be problematic for the model as it will have a hard time prioritizing variables. However, to find the most important variables in the first place and to check for the performance difference, a model with all variables needs to fitted first. This scenario cannot be generalized and different results may occur for other datasets. Using a model with only a few predictors does not only simplify prediction tasks but also reduces runtime for hyperparameter tuning and performance estimation.

5.4. Variable importance

There are some downsides using the internal variable importance approach of xgboost: Due to the contribution of three different parts to the overall importance score it is complicated to understand why a specific feature was selected. Furthermore the importance calculation approach is only valid for this algorithm and cannot be compared to others. Nevertheless, as we only relied on the variable importance for this specific algorithm, using the internal xgboost approach was sufficient for this work.

It is not surprising that vegetation indices are most important for the model as they are most sensitive to changes in vegetation health. Even though we are not directly looking at vegetation health but using the level of defoliation as a proxy, these indices seem to help the model most deciding whether a tree is defoliated or not. Vegetation indices can help here in two ways: 1) Trees that show a high level of defoliation do also reflect their bad health status through the remaining foliation. 2) Defoliated trees have more influence of bare ground information in their pixel values and will therefore be classified as defoliated by the model.

Even though no NRI made it among the most important variables in this study (stating that the first seven of this study are the most important ones), it is interesting that all ranks from 8 - 30 are occupied by NRI (Figure 4).

Our statement saying that the important indices of this study are the first seven can be seen critical as we only based the selection on a visual inspection of

the variable importance results (Figure 4). The decision to make a cut between rank seven and eight was based on a combination of two facts: 1) Using only vegetation indices is easier for large scale predictions using satellites like Sentinel-2 (most NRI cannot be used with it) and 2) the drop in the importance score of the variable importance results (Figure 4). However, based on this statement, we could also have made the cut between rank five and 6 but including the two vegetation indices at rank six and seven will eventually improve the model and does not increase runtime.

5.5. Spatial prediction

The spatial predictions showed that the model tries to avoid making extreme predictions since most values ranged between 30 % and 80 %. This behavior is mainly triggered by the conentration of the model on the distribution of defoliation in the *Laukiz 1*, *Luiando* and *Oiartzun* training plots. This focus then causes the high prediction error for *Laukiz 2* for which a lot of defoliation values actually range between 0 % and 20 %. The fitted model would need more training samples for plots that show a similar defoliation as *Laukiz 2* to reach a better performance for similar plots.

6. Conclusion

7. Appendix

Appendix A. Spectral signatures of each plot

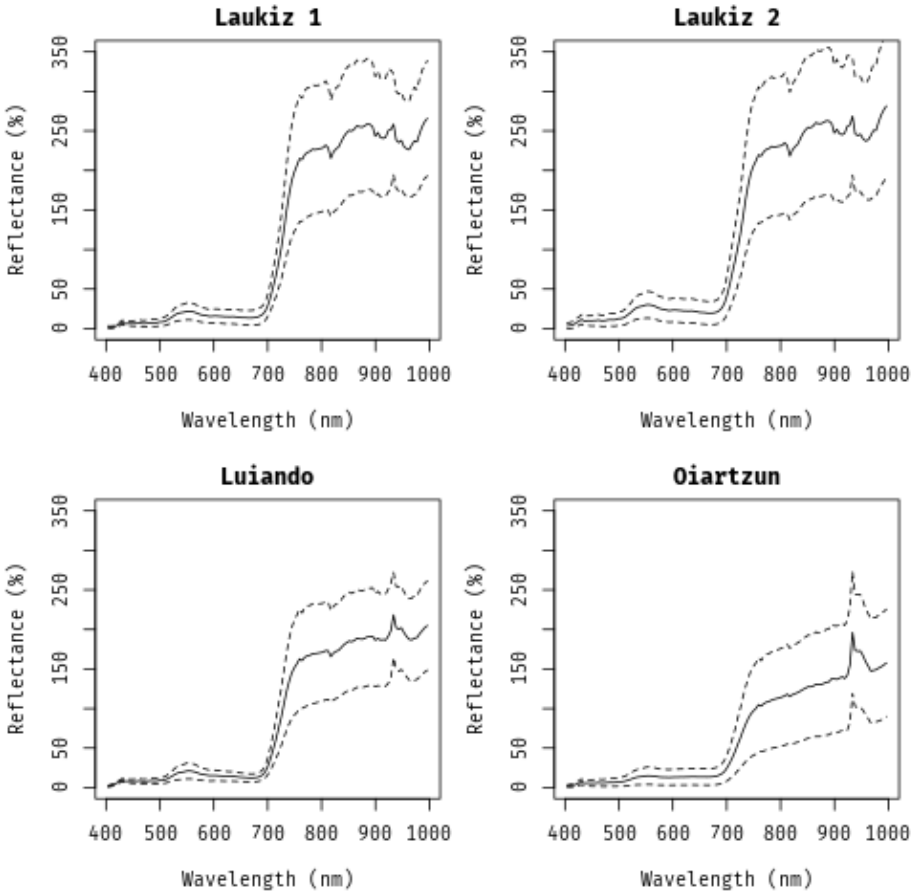

Figure A.7: Spectral signatures (mean and standard deviation) of each plot.

References

Adamczyk, J., & Osberger, A. (2015). Red-edge vegetation indices for detecting and assessing disturbances in Norway spruce dominated mountain forests. *International Journal of Applied Earth Observation and Geoinformation*, *37*, 90–99. doi:10/f64b6c. 00009.

Belgiu, M., & Drăguţ, L. (2016). Random forest in remote sensing: A review of applications and future directions. *ISPRS Journal of Photogrammetry and Remote Sensing*, *114*, 24–31. doi:10/f8ndk8. 00281.

Bergstra, J., & Bengio, Y. (2012). Random Search for Hyper-parameter Optimization. *J. Mach. Learn. Res.*, *13*, 281–305.

Bischl, B., Lang, M., Kotthoff, L., Schiffner, J., Richter, J., Studerus, E., Casalicchio, G., & Jones, Z. M. (2016). mlr: Machine learning in R. *Journal of Machine Learning Research*, *17*, 1–5.

Bischl, B., Richter, J., Bossek, J., Horn, D., Thomas, J., & Lang, M. (2017). mlrMBO: A Modular Framework for Model-Based Optimization of Expensive Black-Box Functions. *ArXiv e-prints*, . arXiv:1703.03373.

Breiman, L. (2001). Random Forests. *Machine Learning*, *45*, 5–32. doi:10/d8zjwq.

Brenning, A. (2012). Spatial cross-validation and bootstrap for the assessment of prediction rules in remote sensing: The R package sperrorest. In *2012 IEEE International Geoscience and Remote Sensing Symposium*. IEEE. doi:10.1109/igarss.2012.6352393 R package version 2.1.0.

Chen, T., & Guestrin, C. (2016). XGBoost: A Scalable Tree Boosting System. In *Proceedings of the 22Nd ACM SIGKDD International Conference on Knowledge Discovery and Data Mining* KDD '16 (pp. 785–794). New York, NY, USA: ACM. doi:10.1145/2939672.2939785 01130.

Friedman, J., Hastie, T., & Tibshirani, R. (2010). Regularization Paths for Generalized Linear Models via Coordinate Descent. *Journal of Statistical Software*, *33*, 1–22. 05097.

Ganley, R. J., Watt, M. S., Manning, L., & Iturritxa, E. (2009). A global climatic risk assessment of pitch canker disease. *Canadian Journal of Forest Research*, *39*, 2246–2256. doi:10/bmj3nk. 00053.

Huete, A. R., Liu, H. Q., Batchily, K., & van Leeuwen, W. (1997). A comparison of vegetation indices over a global set of TM images for EOS-MODIS. *Remote Sensing of Environment*, *59*, 440–451. doi:10/bgtpgv. 01474.

Hutter, F., Hoos, H. H., & Leyton-Brown, K. (2011). Sequential Model-Based Optimization for General Algorithm Configuration. In *Lecture Notes in Computer Science* (pp. 507–523). Springer Berlin Heidelberg. doi:10.1007/978-3-642-25566-3_40 00678.

Iturritxa, E., Mesanza, N., & Brenning, A. (2014). Spatial analysis of the risk of major forest diseases in Monterey pine plantations. *Plant Pathology*, *64*, 880–889. doi:10/gdq9pb.

Iturritxa, E., Trask, T., Mesanza, N., Raposo, R., Elvira-Recuenco, M., & Patten, C. L. (2017). Biocontrol of Fusarium circinatum Infection of Young Pinus radiata Trees. *Forests*, *8*, 32. doi:10/f9t3d8. 00000.

Jiang, Y., Wang, T., de Bie, C. A. J. M., Skidmore, A. K., Liu, X., Song, S., Zhang, L., Wang, J., & Shao, X. (2014). Satellite-derived vegetation indices contribute significantly to the prediction of epiphyllous liverworts. *Ecological Indicators*, *38*, 72–80. doi:10/f5q4b4. 00018.

Jones, D. R., Schonlau, M., & Welch, W. J. (1998). Efficient global optimization of expensive black-box functions. *Journal of Global Optimization*, *13*, 455–492. doi:10/fg68nc.

Karatzoglou, A., Smola, A., Hornik, K., & Zeileis, A. (2004). Kernlab – An S4 Package for Kernel Methods in R. *Journal of Statistical Software*, *11*, 1–20. doi:10/gdq9pc. R package version 0.9-25.

Lary, D. J., Alavi, A. H., Gandomi, A. H., & Walker, A. L. (2016). Machine learning in geosciences and remote sensing. *Geoscience Frontiers*, *7*, 3–10. doi:10/f79ddn. 00069.

Lehnert, L. W., Meyer, H., & Bendix, J. (2018). *Hsdar: Manage, Analyse and Simulate Hyperspectral Data in R*. 00012 R package version 0.7.1.

Lelong, C. C. D., Roger, J.-M., Brégand, S., Dubertret, F., Lanore, M., Sitorus, N. A., Raharjo, D. A., & Caliman, J.-P. (2010). Evaluation of Oil-Palm Fungal Disease Infestation with Canopy Hyperspectral Reflectance Data. *Sensors*, *10*, 734–747. doi:10/bb8wm6. 00045.

Lu, D., Chen, Q., Wang, G., Liu, L., Li, G., & Moran, E. (2016). A survey of remote sensing-based aboveground biomass estimation methods in forest ecosystems. *International Journal of Digital Earth*, *9*, 63–105. doi:10/gdthzv. 00111.

Martinez del Castillo, E., García-Martin, A., Longares Aladrén, L. A., & de Luis, M. (2015). Evaluation of forest cover change using remote sensing techniques and landscape metrics in Moncayo Natural Park (Spain). *Applied Geography*, *62*, 247–255. doi:10/gdthzt. 00029.

Mesanza, N., Iturritxa, E., & Patten, C. L. (2016). Native rhizobacteria as biocontrol agents of Heterobasidion annosum s.s. and Armillaria mellea infection of Pinus radiata. *Biological Control*, *101*, 8–16. doi:10/f8xnp3. 00004.

Michez, A., Piégay, H., Lisein, J., Claessens, H., & Lejeune, P. (2016). Classification of riparian forest species and health condition using multi-temporal and hyperspatial imagery from unmanned aerial system. *Environmental Monitoring and Assessment*, *188*, 146. doi:10/f8q9wp. 00037.

Probst, P., Wright, M., & Boulesteix, A.-L. (2018). Hyperparameters and Tuning Strategies for Random Forest. *ArXiv e-prints*, . arXiv:1804.03515. 00000.

R Core Team (2017). *R: A Language and Environment for Statistical Computing*. Vienna, Austria. 88058 R version 3.4.4.

Sexton, J. O., Noojipady, P., Anand, A., Song, X.-P., McMahon, S., Huang, C., Feng, M., Channan, S., & Townshend, J. R. (2015). A model for the propagation of uncertainty from continuous estimates of tree cover to categorical forest cover and change. *Remote Sensing of Environment*, *156*, 418–425. doi:10/f6v7zc. 00038.

Sims, D. A., & Gamon, J. A. (2002). Relationships between leaf pigment content and spectral reflectance across a wide range of species, leaf structures and developmental stages. *Remote Sensing of Environment*, *81*, 337–354. doi:10/fb9nnj. 01985.

Sinha, S., Jeganathan, C., Sharma, L. K., & Nathawat, M. S. (2015). A review of radar remote sensing for biomass estimation. *International Journal of Environmental Science and Technology*, *12*, 1779–1792. doi:10/gdthzw. 00043.

Vapnik, V. (1998). The support vector method of function estimation. In *Nonlinear Modeling* (pp. 55–85). Springer US. doi:10.1007/978-1-4615-5703-6_3.

Wu, C., Niu, Z., Tang, Q., & Huang, W. (2008). Estimating chlorophyll content from hyperspectral vegetation indices: Modeling and validation. *Agricultural and Forest Meteorology*, *148*, 1230–1241. doi:10/dhcp6r.

Zarco-Tejada, P. J., Pushnik, J. C., Dobrowski, S., & Ustin, S. L. (2003). Steady-state chlorophyll a fluorescence detection from canopy derivative reflectance and double-peak red-edge effects. *Remote Sensing of Environment*, *84*, 283–294. doi:10/c8gjtt. 00238.

Zhang, K., Thapa, B., Ross, M., & Gann, D. (2016). Remote sensing of seasonal changes and disturbances in mangrove forest: A case study from South Florida. *Ecosphere*, (p. e01366). doi:10.1002/ecs2.1366@10.1002/(ISSN)2150-8925.ExtremeColdSpells.